DIFFERENTIAL MICROPHONE ARRAYS FOR THE UNDERWATER ACOUSTIC CHANNEL

Rotem Mulayoff, Yaakov Buchris, and Israel Cohen

Technion, Israel Institute of Technology, Technion City, Haifa 32000, Israel
{smulayof@,bucris@campus, icohen@ee}.technion.ac.il

ABSTRACT

Design of underwater acoustic sensing and communication systems is a very challenging task due to several channel effects like multipath propagation and Doppler spread. In order to cope with these effects, beamforming techniques have been applied to the design of such systems. The broadband nature of acoustic systems motivates the use of beamformers with frequency-invariant beampattern. Moreover, in some cases, these systems are limited by their physical dimensions. Differential microphone arrays (DMAs) beamformers, which have been used extensively in recent years for broadband audio signals, may comply with these requirements. DMAs are small-size arrays which can provide almost frequency-invariant beampatterns and high directivity. In this paper, we present a pool experiment which shows the compatibility of DMAs for the underwater acoustic channel. Additionally, we show how to compensate for the array mismatch errors leading to much better performance level and robust beamformers.

Index Terms— Underwater acoustic channel, differential microphones, broadband beamforming, array mismatch errors.

1. INTRODUCTION

In the last several decades, underwater acoustic communication and acoustic sensing became essential for several real-world applications, both commercial and military [1]. To name a few, oil drilling, laying cable and gas pipeline on the seabed, are some of the important commercial applications. In military applications, we can indicate the underwater warfare via submarines, commando operations, and many more. Numerous devices were developed throughout the years to fill the needs of these applications like Sound Navigation and Ranging (SONAR), Remotely Operated Vehicle (ROV), Underwater communication systems, and others.

Design of underwater acoustic devices for the underwater environment is very challenging due to the underwater acoustic channel which is characterized as a time-varing spatially uncorrelated fading channel. It introduces several effects like frequency-dependent acoustic attenuation, Doppler effect, ambient noise, and directional noise like machinery and propeller cavitation noise of nearby vessels. Typically, the underwater acoustic signals are broadband in nature [2] as a result of attenuation that increases with the frequency. Therefore, when designing beamformers for underwater acoustic systems, it is desirable to design them with frequency-invariant beampatterns. Additionally, since in some of the systems the beamformers are integrated into small payloads, the apertures of the arrays should be compact.

This research was supported by the Israel Science Foundation (grant no. 576/16), Qualcomm Research Fund and MAFAAT-Israel Ministry of Defense.

One of a well-known family of frequency-invariant beamformers is the differential microphone arrays (DMAs), originally applied to speech signals [3–9]. DMAs refer to arrays that combine closely spaced sensors to respond to the spatial derivatives of the acoustic pressure field. These small-size arrays yield nearly frequency-invariant beampatterns, and include the superdirective beamformer [10] as a particular case.

In this paper, we apply the DMAs concept to the underwater acoustic channel. We present a pool experiment which proves the feasibility of DMAs for the underwater acoustic environment. The array was constructed from omni-directional hydrophones and therefore was uncalibrated. As a consequence, essential part of the decoding process deals with estimation and compensation of array mismatch errors like gain and phase errors. The results show that DMAs can be utilized for the underwater acoustic environment and may provide small-size frequency-invariant robust beamformers.

2. SIGNAL MODEL

We consider an underwater acoustic source signal, $X(\omega)$, that propagates in an anechoic underwater acoustic channel at the speed of sound, i.e., $c \approx 1500\mathrm{m/s}$, and impinges on a uniform linear array of M sensors, where the distance between two successive sensors is equal to δ. The direction of $X(\omega)$ to the array is denoted by the azimuth angle θ. Assuming a far-field propagation, the time delay between the mth microphone and the first microphone is $(m-1)\frac{\delta}{c}\cos\theta$. Therefore, the mth microphone signal is [7]

$$Y_m(\omega) = e^{-j(m-1)\omega\frac{\delta}{c}\cos\theta}X(\omega) + V_m(\omega), \tag{1}$$

where $j = \sqrt{-1}$, $\omega = 2\pi f$ is the angular frequency, $f > 0$ is the temporal frequency and $V_m(\omega)$ is the additive noise at the mth microphone. In a vector form, (1) becomes

$$\mathbf{y}(\omega) = [Y_1(\omega) \quad \cdots \quad Y_M(\omega)]^T = \mathbf{d}(\omega,\theta)X(\omega) + \mathbf{v}(\omega), \tag{2}$$

where ^{T} denotes the transpose operator, and

$$\mathbf{d}(\omega,\theta) = \left[1 \quad e^{-j\omega\frac{\delta}{c}\cos\theta} \quad \cdots \quad e^{-j(M-1)\omega\frac{\delta}{c}\cos\theta}\right]^T \tag{3}$$

is the steering vector. The vector $\mathbf{v}(\omega)$ is defined similarly to $\mathbf{y}(\omega)$. According to the DMA model, it is assumed that the desired signal arrives from the direction $\theta = 0^\circ$, and the acoustic wavelength $\lambda = c/f$ is much larger than the element spacing, δ, i.e., $\lambda \gg \delta$, to approximate the differential of the pressure signal.
In order to design the beamformer, the signal of each microphone is multiplied by a complex gain $H_m(\omega), m = 1, 2, ..., M$, and the beamformer output signal is

$$Z(\omega) = \sum_{m=1}^{M} H_m^*(\omega)Y_m(\omega) = \mathbf{h}^H(\omega)\mathbf{y}(\omega), \tag{4}$$

where the superscript * denotes the complex conjugate operator, ^{H} denotes the Hermitian operator, and $\mathbf{h}(\omega)$ is defined as

$$\mathbf{h}(\omega) = [H_1(\omega) \quad H_2(\omega) \quad \cdots \quad H_M(\omega)]^T. \tag{5}$$

The beampattern of a given beamformer $\mathbf{h}(\omega)$ is defined as

$$\mathcal{B}[\mathbf{h}(\omega), \theta] = \mathbf{h}^H(\omega)\mathbf{d}(\omega, \theta). \tag{6}$$

The theoretical frequency-invariant beampattern of an Nth-order DMA is given as [3]

$$\mathcal{B}_N(\theta) = \sum_{n=0}^{N} a_{N,n} \cos^n(\theta), \tag{7}$$

where $\{a_{N,n}\}_{n=0}^{N}$ are real coefficients. An Nth-order DMA can be designed using at least $M = N + 1$ sensors, satisfying N attenuation constraints and one distortionless constraint. Taking $M > N + 1$ may lead to a more robust beamformer [8], but in this work we will concentrate on the case of $M = N + 1$. Figure. 1 presents examples of (7) for the case of $N = 1, 2, 3$.

Following the approach suggested at [7] for design of DMAs, we can design a DMA beamformer with a desired beampattern by solving the linear system:

$$\mathbf{D}(\omega, \boldsymbol{\theta})\mathbf{h}(\omega) = \boldsymbol{\beta}, \tag{8}$$

where

$$\boldsymbol{\theta} = [0 \quad \theta_1 \quad \cdots \quad \theta_{M-1}]^T \tag{9}$$

$$\boldsymbol{\beta} = [1 \quad \beta_1 \quad \cdots \quad \beta_{M-1}]^T, \tag{10}$$

$\{\theta_m\}_{m=1}^{M-1}$ are set of angles according to the desired theoretical beampattern, $\{\beta_m\}_{m=1}^{M-1}$ are the values of $\mathcal{B}_N(\theta)$ at the directions specified by $\boldsymbol{\theta}$, and the matrix $\mathbf{D}(\omega, \boldsymbol{\theta})$ is a $M \times M$ matrix given by

$$\mathbf{D}(\omega, \boldsymbol{\theta}) = \begin{bmatrix} \mathbf{d}^H(\omega, 0) \\ \mathbf{d}^H(\omega, \theta_1) \\ \vdots \\ \mathbf{d}^H(\omega, \theta_{M-1}) \end{bmatrix}. \tag{11}$$

From (8) we can derive the beamformer vector

$$\mathbf{h}(\omega) = \mathbf{D}^{-1}(\omega, \boldsymbol{\theta})\boldsymbol{\beta}. \tag{12}$$

It can be shown that the beampattern achieved by this method is approximately frequency-invariant. This fact may be exploited for the underwater scenario.

3. EXPERIMENTAL SETUP & COURSE

In this section, we present a detailed description of an experiment aimed to test the potential of DMAs for the underwater scenario. The experiment took place in a measurement pool at RAFAEL Ltd, Haifa. The measurements pool is 10 meters high, 20 meters long, and 10 meters wide. We used one omni-directional hydroacoustic projector as the transmitting source. The transmitter model was D11BB manufactured by NEPTUNE Ltd with roughly flat Transmit Voltage Response (TVR) of $150\text{dB re } 1\mu\text{Pa/V@1m}$ at the relevant frequencies. The transmitter was deployed at 5 meters depth. Using this transmitter we broadcasted broadband signals with 2kHz bandwidth around 10kHz central frequency.

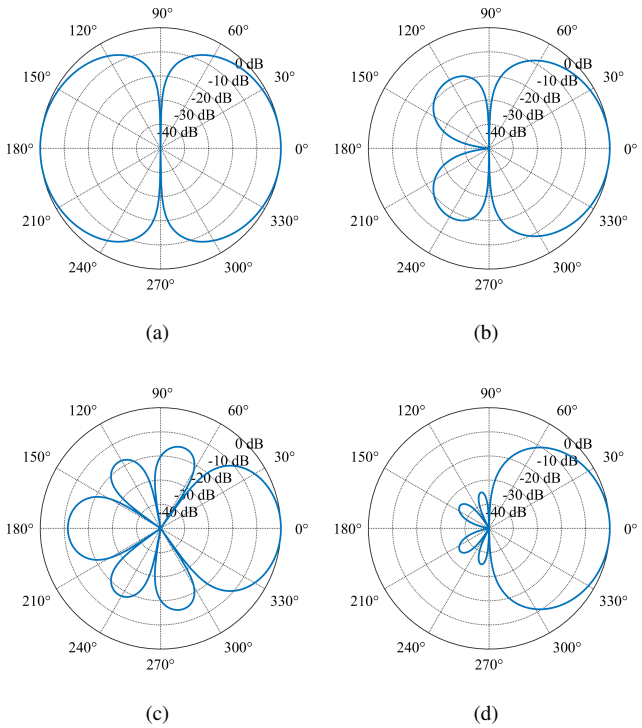

Figure 1: Theoretical beampatterns produced by (7): (a) First-order dipole with a single null at 90^0, (b) second-order cardioid with nulls at 90^0 and 180^0, (c) third-order hypercardioid with nulls at 55^0, 100^0 and 145^0, (d) third-order pattern with nulls at 90^0, 120^0, and 180^0.

To construct the microphone array, we used $M = 4$ similar hydrophones model TC4034 manufactured by Teledyne RESON Ltd, with flat Open-Circuit Voltage (OCV) sensitivity in the relevant frequencies of approximately $-216\text{dB re}1\text{V}/\mu\text{Pa@1m}$. Additionally, we self-manufactured a mounting base for the linear array by drilling in a wood board four holes equally spaced and roughly aligned with element spacing of $\delta \approx 2$ cm. After that, we placed the hydrophones inside the holes to form a linear microphone array. The cables were ground shielded to prevent signal leakage between the sensors. The final product can be seen in Fig. 2.

We connected the array to a rod and deployed it 5 meters deep into the water, and approximately 6 meters away from the source. This distance ensures that we are in the far-field of the source, and the incoming waves are approximately plane waves. The dry part of the rod was placed in a protractor to record the array angle with respect to the source. During the experiment we scanned the array by rotating it from the endfire direction (i.e., $\theta = 0^\circ$) in steps of 2 degrees, up to $\theta = 180^\circ$, and recorded the received signals. The other side (i.e., from $\theta = 180^\circ$ to $\theta = 360^\circ$) is symmetric and thus was not recorded. Figure. 3 illustrates this structure.

In this setup, reflections from the water surface and the side walls of the pool can also be received by the array. These echoes impacting the beamformer in many directions, especially not in the angle that we are aiming for, and thus they can distort the measured beampattern. Therefore, we located this setup in the center of the pool, and transmitted broadband pulses with short durations that

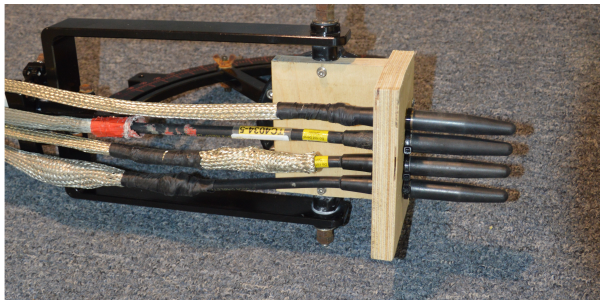

Figure 2: The constructed microphone array of $M = 4$ sensors.

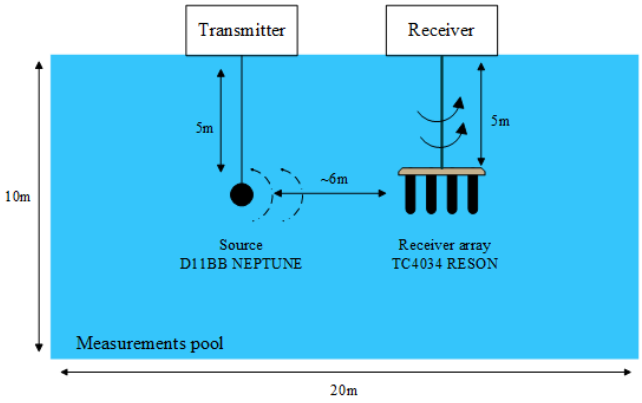

Figure 3: The setup of the experiment.

enabled time separation between the direct path and its reflections.

Throughout the experiment we sampled the received signals using 2 MHz NI USB-6366 sampler. The sampling was performed simultaneously in all channels and not serially, to cancel additional delays. Furthermore, analog equipment was used to filter and amplify the analog signals.

The underwater sound velocity is known to be strongly influenced by the water temperature, salinity, depth and more [11]. We measured the underwater sound velocity by using probe model SVP 70, manufactured by RESON Ltd. The recorded sound velocity was $c = 1489.13\text{m/sec}$, and we used this value for the processing procedure.

4. DATA ANALYSIS

In this section, we present the decoding process of the recorded data. An essential part of it was to estimate and compensate for array mismatch errors which are the main reason for performance degradation. In the following, we describe and address the model mismatch errors.

The model of the incoming signal specified by (1) assumes a unity gain for each sensor, relative delays due to different propagation distances between different sensors, known and constant element spacing, and a known value of the sound velocity in water. Practically, the signals that have been received by the array's microphone passed through analog equipment such as piezoelectric sensors, analog filters and amplifiers. Each part of this analog chain has a transfer function which can be both sensor and frequency dependent. Moreover, we observed that the gain of the incoming signal depends also on the direction θ. Signals arriving from the endfire are more unevenly gained between the sensors than signals arriving from the broadside. This effect was caused by the geometry of our setup, due to the large size of the receiving hydrophones with respect to the wavelength. Thus, an extended model of (1) which considers all these mismatch origins can be written as

$$Y_m(\omega,\theta) = a_m(\omega,\theta)e^{-j\omega(\tau_m+\frac{\delta_m}{c}\cos\theta)}X(\omega) + V_m(\omega), \quad (13)$$

where c is the measured velocity, $a_m(\omega,\theta)$ is the gain of the mth sensor which depends both on frequency and θ, τ_m is the analog delay introduced by the mth sensor, and δ_m is the distance between the first sensor and the mth sensor. We assumed for simplicity that the analog chain causes a linear delay between the signals.

Additionally, we neglected the dependency of the gain on the frequency and assumed that $a_m(\omega,\theta) \approx a_m(\theta)$. In the following results we show that such an approximation leads to satisfying results, yet, the consideration of the dependency of the gain on frequency is indeed a topic for future research. Assuming high SNR level, estimation of $a_m(\theta)$ can be done by taking the root-mean-square (RMS) of the corresponding temporal signal $y_m(t,\theta)$ for each direction and sensor. Since we are interested in the gain difference between the sensors, and not in the amplitude of the received signal, we normalized the RMS value of each sensor by the RMS of the reference signal, i.e., $m = 1$. This can be written mathematically as

$$\hat{a}_m(\theta) = \frac{\mathcal{RMS}\{y_m(t,\theta)\}}{\mathcal{RMS}\{y_1(t,\theta)\}}, \quad (14)$$

where for a general signal $v(t)$, the $\mathcal{RMS}\{v(t)\}$ is given by:

$$\mathcal{RMS}\{v(t)\} = \sqrt{\frac{1}{T}\int_0^T v^2(t)dt}. \quad (15)$$

The phase mismatch is estimated from the sampled signals by a two-step algorithm. In the first step we estimate the total time delay between the mth sensor and sensor 1, denoted by $\mathcal{T}_m(\theta)$, for each angle θ in the time domain. Then, in the second step we estimate the values of τ_m and δ_m based on information from the first step. In the first step we used standard correlation method, that is:

$$\hat{\mathcal{T}}_m(\theta) = \arg\max_t \int_{-\infty}^{\infty} y_1(\alpha+t,\theta)y_m(\alpha,\theta)d\alpha. \quad (16)$$

In the second step we look at the following relation:

$$\mathcal{T}_m(\theta) = \tau_m + \frac{\delta_m}{c}\cos\theta, \quad (17)$$

which is a linear relation between $\mathcal{T}_m(\theta)$ and $\cos\theta$. Let $\{\theta_l\}_{l=1}^L$ be the set of measured angels in our experiment. Thus, we have $L \gg 2$ measurements of $\mathcal{T}_m(\theta)$ for each sensor. Using the Least Squares (LS) method we can estimate τ_m and δ_m. The LS estimation is given by:

$$[\hat{\tau}_m,\hat{\delta}_m] = \arg\min_{\tau,\delta}\sum_{l=1}^{L}\|\mathcal{T}_m(\theta_l) - \tau - \frac{\delta}{c}\cos\theta_l\|^2. \quad (18)$$

Finally, in order to compensate the mismatch errors described above, we rewrite (3) as below

$$\hat{\mathbf{d}}(\omega,\theta) = \Big[\hat{a}_1(\theta) \quad \hat{a}_2(\theta)e^{-j\omega(\hat{\tau}_1+\frac{\hat{\delta}_1}{c}\cos\theta)} \quad \dots \quad \hat{a}_M(\theta)e^{-j\omega(\hat{\tau}_M+\frac{\hat{\delta}_M}{c}\cos\theta)}\Big]^T, \quad (19)$$

and thus the beamformer coefficients formula follows:

$$\hat{\mathbf{h}}(\omega) = \hat{\mathbf{D}}^{-1}(\omega, \boldsymbol{\theta})\boldsymbol{\beta} \tag{20}$$

where $\hat{\mathbf{D}}(\omega, \boldsymbol{\theta})$ is constructed similarly to $\mathbf{D}(\omega, \boldsymbol{\theta})$ from $\hat{\mathbf{d}}(\omega, \theta)$.

5. RESULTS

After the calibration process described in the previous section, we used $\hat{\mathbf{h}}(\omega)$ to calculate the beamformer output. Then for each angle we computed the beamformer output signal in the frequency domain as presented in Section 2. Next we calculated the power of the beamformer output signal for each angle. The power levels were normalized so that the maximal power was 0dB. Figure 4 presents the normalized power vs. θ of the four examples presented in Fig. 1. The black dashed line is for the case of using $\hat{\mathbf{h}}(\omega)$, while the blue circles line is obtained by ignoring the mismatch and using $\mathbf{h}(\omega)$ (12). One can see the resemblance of the black dashed line to the original patterns presented in Fig. 1, and also the improvement achieved by taking into account the mismatch errors.

Figure 5 presents the white noise gain (WNG) of the beamformer which is given by

$$\mathcal{W}\left[\mathbf{h}(\omega)\right] = \frac{\left|\mathbf{h}^H(\omega)\mathbf{d}(\omega,\theta_s)\right|^2}{\mathbf{h}^H(\omega)\mathbf{h}(\omega)}. \tag{21}$$

Figure 6 presents the directivity factor (DF) which is given by

$$\mathcal{D}\left[\mathbf{h}(\omega)\right] = \frac{\left|\mathbf{h}^H(\omega)\mathbf{d}(\omega,\theta_s)\right|^2}{\mathbf{h}^H(\omega)\boldsymbol{\Gamma}_{\mathrm{dn}}(\omega)\mathbf{h}(\omega)}, \tag{22}$$

where $\left[\boldsymbol{\Gamma}_{\mathrm{dn}}(\omega)\right]_{ij} = \mathrm{sinc}\left[\frac{\omega}{c}(\hat{\delta}_j - \hat{\delta}_i)\right]$. In both figures, the red solid line represents the theoretical value where no mismatch errors exist, while the blue dashed line is obtained by using $\hat{\mathbf{h}}(\omega)$. It can be seen that the proposed beamformer provides near optimal results. We also note that the relatively constant value of the DF implies that the beamformer is approximately frequency invariant as we expected. The above results of the WNG and DF are for the case of a first-order dipole, yet, similar results were obtained also for the other patterns in Fig. 1.

These results show the compatibility of DMA beamforming for the underwater acoustic channel. The results are quite satisfying and even expected to improve by considering more accurate models for errors mismatch like frequency dependent gains. Moreover, errors originating from the fact that sensors are not aligned and errors due to the physical size of the sensors were not addressed at all.

6. CONCLUSION

We have applied the concept of DMA beamforming for the underwater acoustic channel. To prove its feasibility, we conducted a pool experiment and transmitted broadband signals via the underwater medium which were received by a DMA of four sensors. This array was built with off-the-shelf hydrophones and therefore several mismatched errors were introduced. We presented a practical algorithm which deals with these errors and provided better results. The results prove the compatibility of DMAs for underwater devices involving broadband signals.

7. ACKNOWLEDGMENT

The authors would like to thank the engineers at the signal processing and algorithm department in RAFAEL Ltd. Especially Jilbert Abitbol and Gilad Avrashi who made this experiment possible.

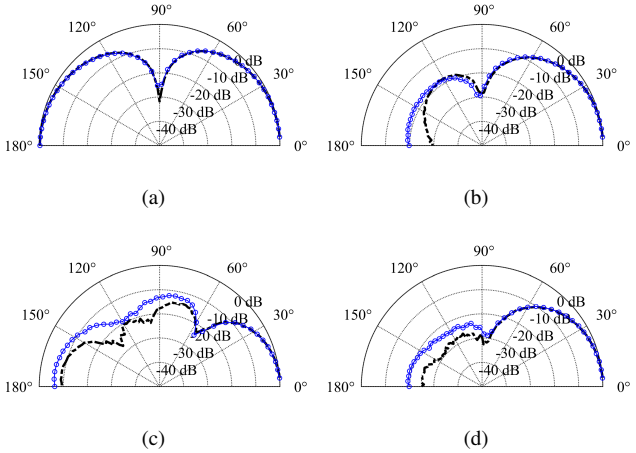

Figure 4: Normalized measured power of the four shapes presented in Fig. 1: (a) First-order dipole with a single null at 90^0, (b) second-order cardioid with nulls at 90^0 and 180^0, (c) third-order hypercardioid with nulls at 55^0, 100^0 and 145^0, (d) third-order pattern with nulls at 90^0, 120^0, and 180^0. The black dashed line is the beampattern achieved by using $\hat{\mathbf{h}}(\omega)$ and the blue circles line is the beampattern achieved by using $\mathbf{h}(\omega)$.

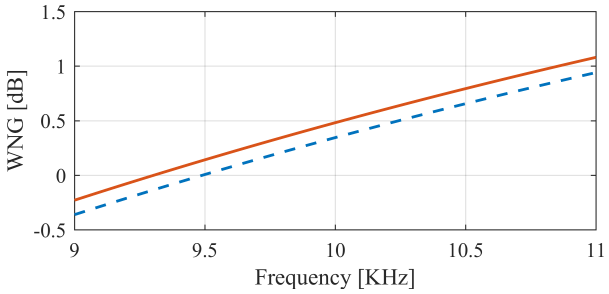

Figure 5: WNG vs. frequency for the first-order dipole. The red solid line is the theoretical value, while the blue dashed line is the proposed beamformer.

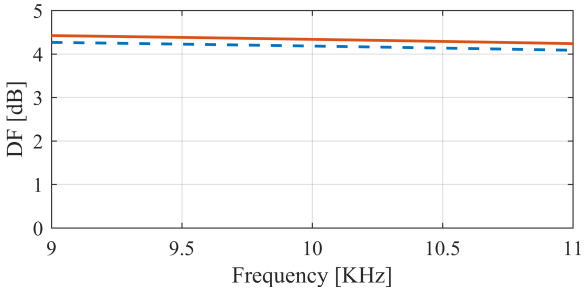

Figure 6: DF vs. frequency for the first-order dipole. The red solid line is the theoretical value, while the blue dashed line is the proposed beamformer.

8. REFERENCES

[1] I. F. Akyildiz, D. Pompili, and T. Melodia, "Underwater acoustic sensor networks: research challenges," *Ad Hoc Net-*

woeks Journal, pp. 257–279, March 2005.

[2] M. Stojanovic and J. Preisig, "Underwater acoustic communication channels: Propagation models and statistical characterization," *IEEE Commun. Mag.*, pp. 84–89, Jan. 2009.

[3] G. W. Elko, "Superdirectional microphone arrays," in *Acoustic Signal Processing for Telecommunication*, S. L. Gay and J. Benesty, Eds. Boston, MA: Kluwer Academic Publishers, 2000, ch. 10, pp. 181–237.

[4] G. W. Elko and A. T. N. Pong, "A simple first-order differential microphone," in *Proc. IEEE Workshop Applicat. Signal Process. Audio Acoust. (WASPAA)*, 1995, pp. 169–172.

[5] M. Buck, "Aspects of first-order differential microphone arrays in the presence of sensor imperfections," *European Trans. Telecommunications*, vol. 13, pp. 115–122, Mar. 2002.

[6] E. De Sena, H. Hacihabiboğlu, and Z. Cavetković, "On the design and implementation of higher order differential microphones," *IEEE Trans. Audio, Speech, Language Process.*, vol. 20, no. 1, pp. 162–174, Jan. 2012.

[7] J. Benesty and J. Chen, *Study and Design of Differential Microphone Arrays*. Berlin, Germany: Springer-Verlag, 2012.

[8] L. Zhao, J. Benesty, and J. Chen, "Design of robust differential microphone arrays," *IEEE Trans. Audio, Speech, Language Process.*, vol. 22, no. 10, pp. 1455–1464, Oct. 2014.

[9] C. Pan, J. Chen, and J. Benesty, "Theoretical analysis of differential microphone array beamforming and an improved solution," *IEEE Trans. Audio, Speech, Language Process.*, vol. 23, no. 11, pp. 2093–2105, Nov. 2015.

[10] H. Cox, R. M. Zeskind, and T. Kooij, "Practical supergain," *IEEE Trans. Acoust., Speech, Signal Processing*, vol. ASSP-34, no. 3, pp. 393–398, June 1986.

[11] R. J. Urick, *Principles of underwater sound*. McGraw-Hill, 1983.